Geophysical Research Letters

RESEARCH LETTER
10.1029/2022GL098756

Key Points:

- Isotopic and thermodynamic modeling results indicate that Gongga-Zheduo granitic rocks in eastern Tibet are sourced from the local crust
- No crustal materials from central Tibet are observed in eastern Tibet arguing against the large-scale crustal flow model
- Cenozoic episodic magmatism in eastern Tibet with a repeated vertical shifting of sources is correlated with staged crustal uplift

Supporting Information:

Supporting Information may be found in the online version of this article.

Correspondence to:
F. Hu,
hufangyang@mail.iggcas.ac.cn

Citation:
Hu, F., Wu, F.-Y., Ducea, M. N., Chapman, J. B., & Yang, L. (2022). Does large-scale crustal flow shape the eastern margin of the Tibetan Plateau? Insights from episodic magmatism of Gongga-Zheduo granitic massif. *Geophysical Research Letters*, *49*, e2022GL098756. https://doi.org/10.1029/2022GL098756

Received 17 MAR 2022
Accepted 10 JUN 2022

Author Contributions:
Conceptualization: Fangyang Hu, Fu-Yuan Wu
Funding acquisition: Fangyang Hu, Fu-Yuan Wu, Mihai N. Ducea
Investigation: Fangyang Hu, Lei Yang
Software: Fangyang Hu
Writing – original draft: Fangyang Hu
Writing – review & editing: Mihai N. Ducea, James B. Chapman

Does Large-Scale Crustal Flow Shape the Eastern Margin of the Tibetan Plateau? Insights From Episodic Magmatism of Gongga-Zheduo Granitic Massif

Fangyang Hu[1,2,3], Fu-Yuan Wu[2,4,5], Mihai N. Ducea[3,6], James B. Chapman[7], and Lei Yang[8]

[1]Key Laboratory of Mineral Resources, Institute of Geology and Geophysics, Chinese Academy of Sciences, Beijing, China, [2]Innovation Academy for Earth Science, Chinese Academy of Sciences, Beijing, China, [3]Department of Geosciences, University of Arizona, Tucson, AZ, USA, [4]State Key Laboratory of Lithospheric Evolution, Institute of Geology and Geophysics, Chinese Academy of Sciences, Beijing, China, [5]College of Earth and Planetary Sciences, University of Chinese Academy of Sciences, Beijing, China, [6]Faculty of Geology and Geophysics, University of Bucharest, Bucharest, Romania, [7]Department of Geology and Geophysics, University of Wyoming, Laramie, WY, USA, [8]College of Earth Sciences, Chengdu University of Technology, Chengdu, China

Abstract The mechanisms driving crustal deformation and uplift of orogenic plateaus are fundamental to continental tectonics. Large-scale crustal flow has been hypothesized to occur in eastern Tibet, but it remains controversial due to a lack of geologic evidence. Geochemical and isotopic data from Cenozoic igneous rocks in the eastern Tibet-Gongga-Zheduo intrusive massif, provide a way to test this model. Modeling results suggest that Cenozoic magmas originated at depths of ~30–40 km, the depth that crustal flow has been postulated to occur at. Detailed isotopic analyses indicate that the igneous rocks are derived from partial melting of the local Songpan-Ganzi crust, arguing against a long-distance crustal flow. Episodic magmatism during the Cenozoic showing a repeated shifting of magmatic sources can be correlated with crustal uplift. The continued indentation of the Indian Block and upwelling of the asthenosphere contribute to the crustal deformation, magmatism, and uplift.

Plain Language Summary How the Tibetan Plateau grows outward and deformed remains controversial. A large-scale crustal flow model has been favored for the expansion of the southeast Tibetan Plateau, arguing that crustal materials could flow hundreds of km resulting in crustal thickening and uplift. Detailed geochemical and isotopic investigations on the largest intrusion (Gongga-Zheduo) in the eastern margin of the Tibetan Plateau show that their magmatic source is local crustal rocks of the Songpan-Ganzi terrane without the input of crustal materials from central Tibet. Thermodynamic and trace element modeling results show that the Cenozoic magma is derived from ~30 to 40 km depth, similar to the depth of postulated crustal flow. The results are inconsistent with the large-scale eastward crustal flow model. A repeated shifting of magmatic sources during the Cenozoic is correlated with crustal uplift. Mantle-crust interaction plays a primary role in the formation of magmatism and modifying crustal rheology. The continued collision between the Indian and Asian blocks and upwelling of the asthenosphere contribute to the crustal deformation and uplift.

1. Introduction

The Tibetan Plateau was created by the India-Asia continental collision during the Cenozoic and is a natural laboratory to test models of continental tectonics. The mechanisms of crustal deformation, uplift, and outward expansion of the plateau are among the most controversial and unresolved aspects of the collision. The Asian block has experienced relatively diffuse deformation, located far away from the Indo-Asian suture zone (England & Houseman, 1986; England & Molnar, 1997). Some researchers have ascribed crustal thickening and outward expansion of the plateau as a result of escape tectonics along major strike-slip faults (Molnar & Tapponnier, 1975; Tapponnier et al., 2001). Others have proposed that the indentation of India is driving large-scale lower crustal flow and redistributing mass, to cause crustal thickening and outward expansion of the plateau (Clark & Royden, 2000; Royden et al., 1997).

The large-scale (>1,000 km) crustal flow model can explain why there is high topography in the absence of significant crustal shortening and a low topographic gradient along the eastern margin of the Tibetan Plateau (EMTP; Figure 1; Clark & Royden, 2000; Royden et al., 1997; Schoenbohm et al., 2006). The central Tibetan

10.1029/2022GL098756

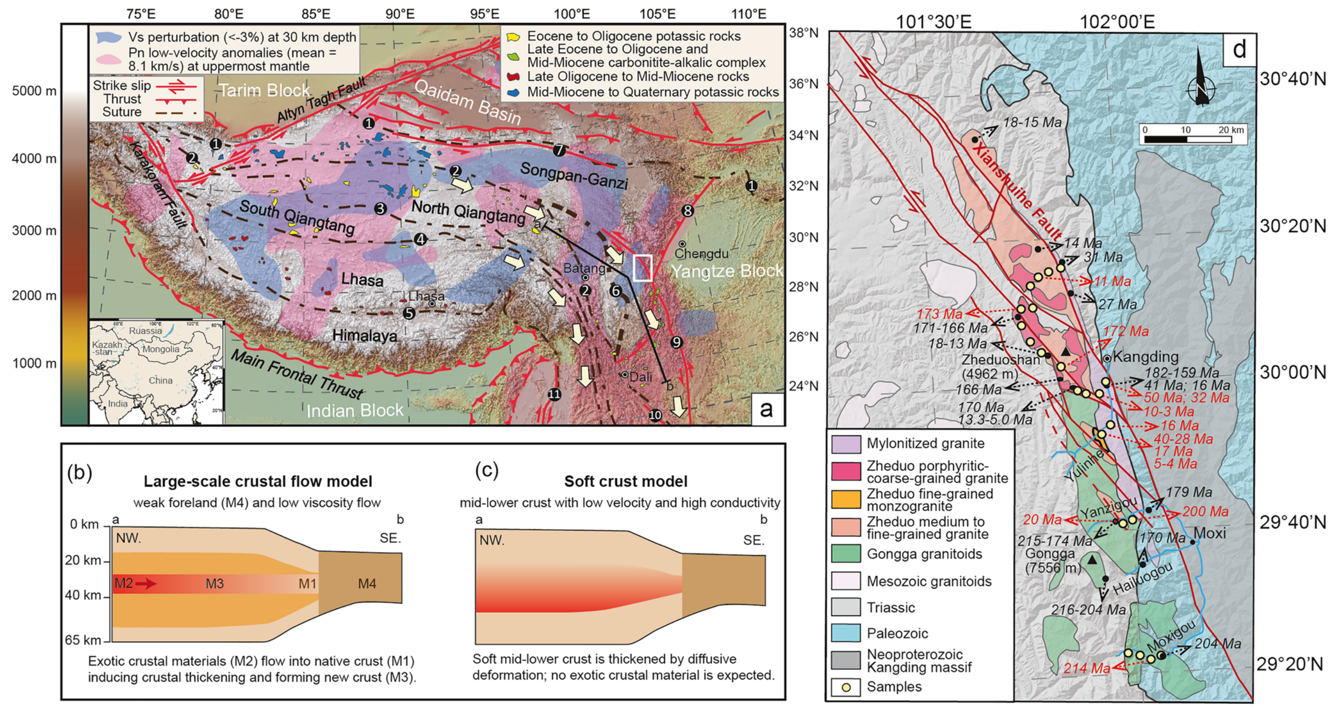

Figure 1. Maps of the Tibetan Plateau and Gongga-Zheduo granitic massif and conceptual models for crustal thickening and tectonic uplift in eastern Tibet. (a) Distribution of geophysical anomalies and Cenozoic magmatic rocks in the Tibetan Plateau. Vs perturbation at 30 km depth are from Y. Yang et al. (2012). Pn low-velocity anomalies at the uppermost mantle are from Zhou and Lei (2016). Light-yellow arrows mark the inferred location of hypothesized flow channels (Bai et al., 2010). The distribution of magmatic rocks is from Chung et al. (2005) and Hou et al. (2006). Numbers represent suture zones and faults: 1-Eastern Kunlun-Animaqing suture zone; 2-Jinshajiang suture zone; 3-Longmuco-Shuanghu suture zone; 4-Bangong-Nujiang suture zone; 5-Indus-Yarlung Zangbo suture zone; 6-Ganzi-Litang suture zone; 7-Kunlun fault; 8-Longmenshan thrust fault; 9-Xianshuihe-Xiaojiang fault; 10-Ailaoshan-Honghe fault; 11-Sagaing fault. (b) Large-scale crustal flow model with crustal thickening caused by channelized exotic crustal materials (after Clark, Bush, et al., 2005; Clark & Royden, 2000). (c) Soft crust model with crustal thickening caused by local crustal diffusive deformation. (d) A simplified geological map of the Gongga-Zheduo granitic massif. Yellow circles denote sample locations. The ages in red are data from this study. The ages in black are from previous studies (Lai & Zhao, 2018; H. Li & Zhang, 2013; H. Li, Zhang, et al., 2015; Searle et al., 2016).

Plateau, with high elevations and thickened crust, provided a lateral pressure gradient required for the crustal flow (Clark & Royden, 2000; Royden et al., 1997). Furthermore, low-velocity and high-conductivity zones with high Poisson's ratios have been reported in the mid-lower crust of the EMTP and Northern Qiangtang terrane (NQT), interpreted to be mobile mid-lower crust (Figure 1; Bai et al., 2010; Bao et al., 2015; Kong et al., 2016; Q. Y. Liu et al., 2014; C.-Y. Wang et al., 2010). Therefore, a crustal flow "channel" was proposed to extend from the NQT to the EMTP, at a depth of ~25–40 km (Figure 1; Bai et al., 2010; Bao et al., 2015; Clark, Bush, et al., 2005; Clark & Royden, 2000).

Crustal flow is a solid-state process (e.g., mylonitic shear zone) that initiates under appropriate stress conditions and when temperatures exceed 400°C–500°C (e.g., Kruse et al., 1991; MacCready et al., 1997; McKenzie et al., 2000). For a large-scale crustal flow (>1,000 km), higher crustal temperatures are required (i.e., >700°C; Kruse et al., 1991). The Tibetan plateau has high modern geothermal gradients (>25°C/km), which are thought to be related to limited erosion and high radiogenic heat production (Whittington et al., 2009). The high heat flow provides a basis for the large-scale crustal flow model and also explains magmatism which involves partial melting of the lower middle crust (H. Li & Zhang, 2013; Searle et al., 2016).

Here, we present a test for the large-scale crustal flow hypothesis in the EMPT using the isotopic signature of magmatic rocks. If large-scale crustal flow from the NQT occurs, distinct isotopic signatures of that terrane are expected in crustal-derived or crustally contaminated melts. The Gongga-Zheduo granitic massif, the largest intrusion in the EMTP, has a complex magmatic history from the Mesozoic (~220–170 Ma) to Cenozoic (~40–5 Ma) (Figure 1; Lai & Zhao, 2018; H. Li & Zhang, 2013; H. Li, Zhang, Zhang, Dong, & Zhu, 2015; Roger et al., 1995; Searle et al., 2016; Y.-Z. Zhang et al., 2017). It provides an opportunity to test the large-scale crustal flow model. Previous studies have tried to use such a method to trace crustal flow in the southern Tibet (e.g., King et al., 2007), but the conclusion was debated because the lower crust of Himalaya has similar isotopic compositions to the Lhasa terrane (e.g., L. Zeng et al., 2011). The Sr-Nd-Hf-O isotopic compositions of the local crust in the EMTP compared to the NQT show clear differences and crustal-derived magmas from the EMTP and NQT can be distinguished (Figure S1 in Supporting Information S1; de Sigoyer et al., 2014; S. Li et al., 2021; Long et al., 2015; Peng et al., 2015; Song et al., 2021; Q. Wang et al., 2016; Y.-C. Zeng et al., 2020; Zhao et al., 2018).

2. Geology of the Gongga-Zheduo Granitic Massif

The Gongga-Zheduo granitic massif (Figure 1) intruded into Triassic turbidites in the Songpan-Ganzi terrane and outcrop along the west side of NNW-SSE trending Xianshuihe Fault. The eastern margin of the massif is an Oligocene mylonite-migmatite zone, intruded by Pliocene dikes (H. Li & Zhang, 2013; Y.-Z. Zhang et al., 2017).

The main part of Gongga-Zheduo massif is subdivided into two units, the Gongga granites in the south and the Zheduo granites in the north (Figure 1). The Gongga granites are mainly composed of Triassic quartz diorite to monzogranite and minor Miocene syenogranite (H. Li, Zhang, et al., 2015). The Zheduo granites consist of mainly Miocene syenogranite with some Jurassic syenogranite (Lai & Zhao, 2018; H. Li, Zhang, et al., 2015; Roger et al., 1995), and newly discovered fine-grained monzogranite and leucogranitic dike (Figures S2–S4 in Supporting Information S1). The Cenozoic magmatism here reflected a complex deformation history related to the Xianshuihe Fault: compression during the Eocene, transition from compression to strike-slip during the Miocene, and large-scale shearing during the Pliocene (e.g., Y. Chen et al., 2020; Y.-Z. Zhang et al., 2017). See Supporting Information for detailed geologic descriptions.

3. Methods

Detailed analytical and modeling methods are presented in the Supporting Information.

3.1. Analytical Methods

Whole-rock major and trace elements were analyzed at the Wuhan Sample Solution Analytical Technology Co., Ltd., Wuhan, China. Zircon U-Pb dating and in situ Sr-Nd-Hf-O isotopic analyses were performed at the Institute of Geology and Geophysics, Chinese Academy of Sciences, Beijing, China.

3.2. Thermodynamic Modeling

Thermodynamic modeling was performed using a Gibbs free energy minimization approach using the software Perple_X (version 6.9.1) to constrain melting temperatures and pressures. The average composition of Neoproterozoic mafic rocks from the western margin of the Yangtze Craton and Paleozoic to Mesozoic metasedimentary rocks from the Songpan-Ganzi terrane were selected as representative of the local EMTP source compositions. A system of Na_2O–CaO–K_2O–FeO–MgO–Al_2O_3–SiO_2–H_2O–TiO_2–O_2 (NCKFMASHTO) and the data set of hp633ver were used for the thermodynamic modeling based on the mineral assemblages and bulk rock compositions, assuming $Fe^{3+}/(Fe^{3+} + Fe^{2+})$ value as 0.2 for basaltic rock and 0.3 for metasedimentary rock, respectively (Forshaw & Pattison, 2021; Pourteau et al., 2020). The water contents are estimated based on the average value of loss-on-ignition. The equilibrium mineral assemblages and melt compositions are exported at discrete *P-T* points for every 10°C and 0.1 GPa using a Perple_X-based program Rcrust (Mayne et al., 2016). The uncertainty of *P-T* estimates are ±1 kbar and ±50°C at the 2-sigma level (Palin et al., 2016).

4. Results and Discussion

4.1. Geochronology of the Gongga-Zheduo Granitic Massif

Our zircon U-Pb dating results indicate that the Gongga-Zheduo granitoid rocks were emplaced from 214 to 4 Ma (Figures S5–S6 in Supporting Information S1, Table S1 in Supporting Information S1), similar to previously published data. There are five main magmatic episodes in the EMTP, which are 215–200 Ma (Gongga monzogranite and leucogranite), 173–172 Ma (Zheduo porphyritic to coarse-grained syenogranite), ~50–30 Ma

(Zheduo fine-grained monzogranite, mylonitized granite and related leucogranite), ~20–10 Ma (Gongga-Zheduo coarse to fine-grained syenogranite), and ~5–3 Ma (Zheduo leucogranite; H. Li & Zhang, 2013; H. Li, Zhang, et al., 2015; Searle et al., 2016; Y.-Z. Zhang et al., 2017).

4.2. Petrogenesis of the Gongga-Zheduo Granitic Massif

Whole-rock geochemistry data and isotopic compositions are listed in Table S2–S5 in Supporting Information S1. All samples are high in SiO_2 (67.6–76.0 wt.%) and most are peraluminous (A/CNK = 0.97–1.11; molar $Al_2O_3/(CaO + Na_2O + K_2O)$) (Figure S7 in Supporting Information S1) and can be divided into two subgroups according to their K_2O/Na_2O ratio (Figure 2). Subgroup 1, including Gongga Triassic leucogranite, Zheduo Jurassic syenogranite, and Gongga-Zheduo Miocene syenogranite, has high K_2O content (4.40–6.98 wt.%) and K_2O/Na_2O ratio (1.22–2.59), and low MgO content (0.11–0.51 wt.%) and Mg# value (Figure 2 and Figure S7 in Supporting Information S1). Subgroup 2, including Gongga Triassic monzogranite, Zheduo Eocene-Oligocene granite, and Zheduo Pliocene leucogranite, has relatively lower K_2O content (1.30–4.53) and K_2O/Na_2O ratio (0.24–1.20), and higher MgO content and Mg# value (0.13–1.32 wt.%; Figure 2 and Figure S7 in Supporting Information S1). Subgroup 1 displays strongly negative Ba, Eu, and Sr anomalies, whereas Subgroup 2 shows negligible or slightly Eu anomalies with enrichment in Ba and Sr (Figure S8 in Supporting Information S1). Subgroup 1 has a high $(La/Yb)_N$ ratio (17.0–264; N denotes the chondrite values from Sun & McDonough, 1989) with a low Sr/Y ratio (4.72–86), in contrast to the Subgroup 2 samples ($(La/Yb)_N$ = 8.09–101; Sr/Y = 26–187; Figure 2). The in situ mineral isotope analyses indicate that Subgroup 1 and Subgroup 2 have distinct isotopic features (Figure 2 and Figure S9 in Supporting Information S1). Subgroup 1 has enriched Sr-Nd-Hf isotopic compositions ($^{87}Sr/^{86}Sr(t) = 0.7083–0.7155$; $\varepsilon_{Nd}(t) = -12.0$ to -3.7; $\varepsilon_{Hf}(t) = -11.2$ to $+3.2$) with elevated zircon $\delta^{18}O$ values (8.2–11.1‰). Subgroup 2 has relative depleted Sr-Nd-Hf isotopic compositions ($^{87}Sr/^{86}Sr(t) = 0.704$ 1–0.7061; $\varepsilon_{Nd}(t) = -8.2$ to $+0.3$; $\varepsilon_{Hf}(t) = -1.0$ to $+7.8$) with mantle-like zircon $\delta^{18}O$ values (4.2–7.3‰), except for the Zheduo Oligocene leucogranite showing slightly enriched isotopic compositions ($^{87}Sr/^{86}Sr(t)$ = 0.707 8–0.7088; $\varepsilon_{Nd}(t) = -8.2$ to -4.2; $\varepsilon_{Hf}(t) = +0.4$ to $+3.1$; $\delta^{18}O$ = 8.0–9.0‰; Figure 2).

Three main petrogenetic models have been proposed for the formation of granitic rocks, including (a) melting of crustal materials (i.e., Patiño Douce, 1999); (b) mixing of crustal-derived melts and mantle-derived melts (i.e., J.-H. Yang et al., 2007); and (c) differentiation of mantle-derived melts (i.e., Castillo, 2012). Our samples have no mafic enclaves and show low MgO content (most <1 wt.%) and Mg# values (<50), suggesting that magma mixing may not have been significant (Figure 2). Their evolved radiogenic isotope values indicate that they did not form by closed-system fractionation of depleted mantle-derived melts. Triassic and Cenozoic shoshonitic rocks are present in the EMTP and have been interpreted to be lithospheric mantle-derived (Q. Chen et al., 2017; Hou et al., 2006; B. Xu et al., 2021). However, these shoshonitic melts cannot produce medium to high-K granitic magma by closed-system fractional crystallization or significant upper crustal assimilation. Subgroup 1 samples have high and uniform $\delta^{18}O$ values, indicating they are sourced from metasedimentary rocks (Figure 2). Subgroup 2 samples show mostly mantle-like $\delta^{18}O$ values (Figure 2), but are felsic, without mafic to intermediate components. Therefore, we interpret the Gongga-Zheduo granitic rocks to have been derived from melting of crust.

The contrasting isotopic and geochemical compositions between Subgroups 1 and 2 indicate that they have different crustal sources. Sr, Nd, and Hf isotopic compositions of Subgroup 1 samples are comparable to Songpan-Ganzi metasedimentary rocks and S-type granites, and lower crustal rocks of NQT (Figure 2). However, their elevated $\delta^{18}O$ values suggest that they are not sourced from the lower crust of NQT (Figure 2; Long et al., 2015; Song et al., 2021; Q. Wang et al., 2016). The isotopic compositions better match the metasedimentary rocks of the Songpan-Ganzi terrane, which are local to the EMTP (Figure 2; de Sigoyer et al., 2014; Roger et al., 1995). Sediment-derived melts at low-pressure exhibit strongly negative Eu anomaly, as well as high La/Yb relative to Sr/Y ratios, reflecting both plagioclase and garnet are residuals (Moyen, 2009; Patiño Douce, 1999; Q. Wang et al., 2016).

The Sr-Nd isotopic compositions of Subgroup 2 samples are more depleted than all crustal materials of NQT (Figure 2), arguing against a derivation from the NQT. Their Sr-Nd-Hf-O isotopic compositions resemble Neoproterozoic mafic rocks from the western margin of Yangtze Craton, which is considered as the basement in the EMTP (de Sigoyer et al., 2014; Zhao et al., 2018). Their high Sr/Y relative to La/Yb ratios without strongly negative Eu anomaly indicates the residual minerals are mainly amphibole and garnet. Hence, we interpret both

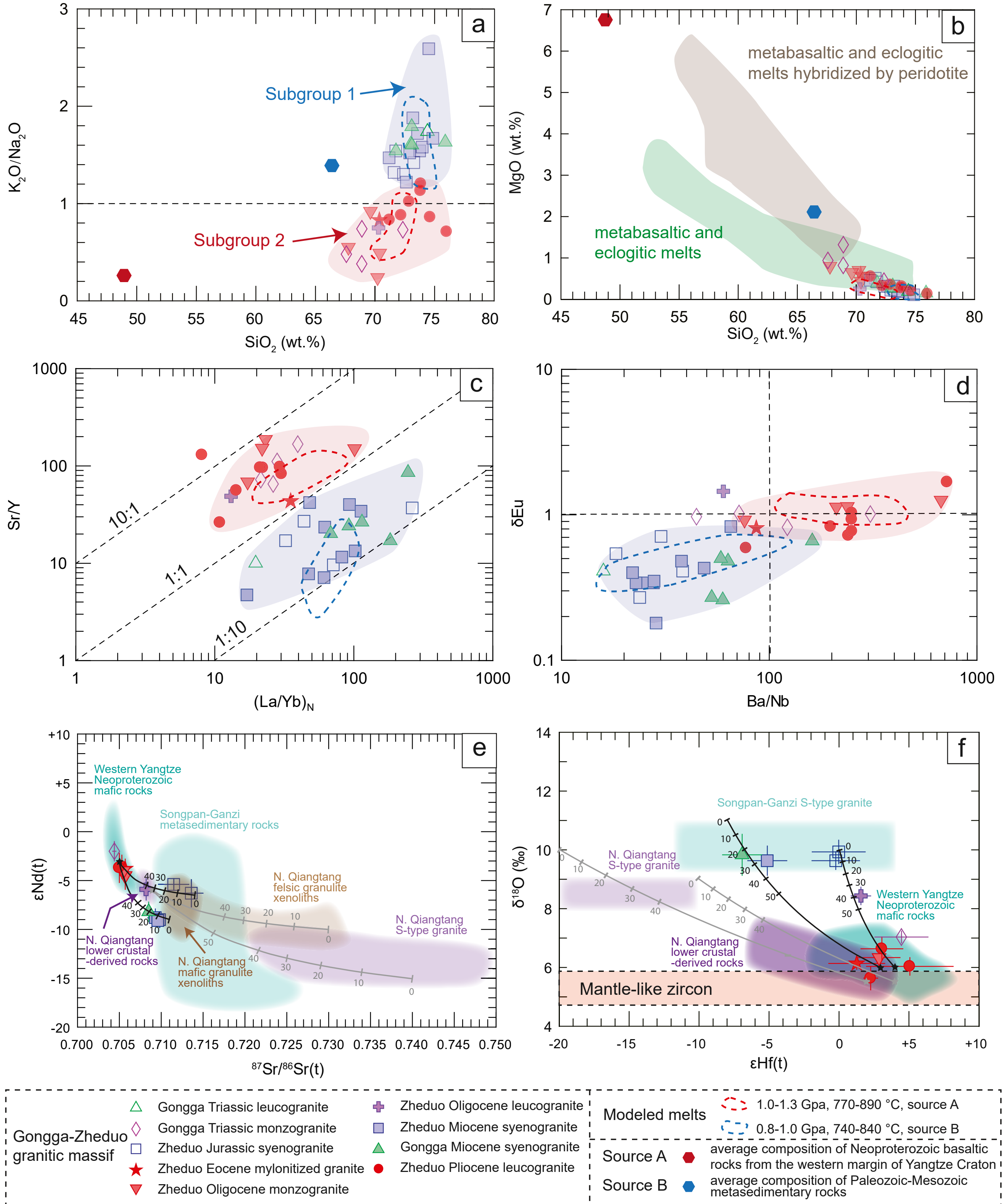
a
Subgroup 1
Subgroup 2
K2O/Na2O
SiO2 (wt.%)
b
metabasaltic and eclogitic melts hybridized by peridotite
metabasaltic and eclogitic melts
MgO (wt.%)
SiO2 (wt.%)
c
10:1
1:1
1:10
Sr/Y
(La/Yb)N
d
δEu
Ba/Nb
e
Western Yangtze Neoproterozoic mafic rocks
Songpan-Ganzi metasedimentary rocks
N. Qiangtang felsic granulite xenoliths
N. Qiangtang S-type granite
N. Qiangtang lower crustal -derived rocks
N. Qiangtang mafic granulite xenoliths
εNd(t)
87Sr/86Sr(t)
f
Songpan-Ganzi S-type granite
N. Qiangtang S-type granite
Western Yangtze Neoproterozoic mafic rocks
N. Qiangtang lower crustal -derived rocks
Mantle-like zircon
δ18O (‰)
εHf(t)
Gongga-Zheduo granitic massif
Gongga Triassic leucogranite
Gongga Triassic monzogranite
Zheduo Jurassic syenogranite
Zheduo Eocene mylonitized granite
Zheduo Oligocene monzogranite
Zheduo Oligocene leucogranite
Zheduo Miocene syenogranite
Gongga Miocene syenogranite
Zheduo Pliocene leucogranite
Modeled melts
1.0-1.3 Gpa, 770-890 °C, source A
0.8-1.0 Gpa, 740-840 °C, source B
Source A
average composition of Neoproterozoic basaltic rocks from the western margin of Yangtze Craton
Source B
average composition of Paleozoic-Mesozoic metasedimentary rocks

Figure 2.

10.1029/2022GL098756

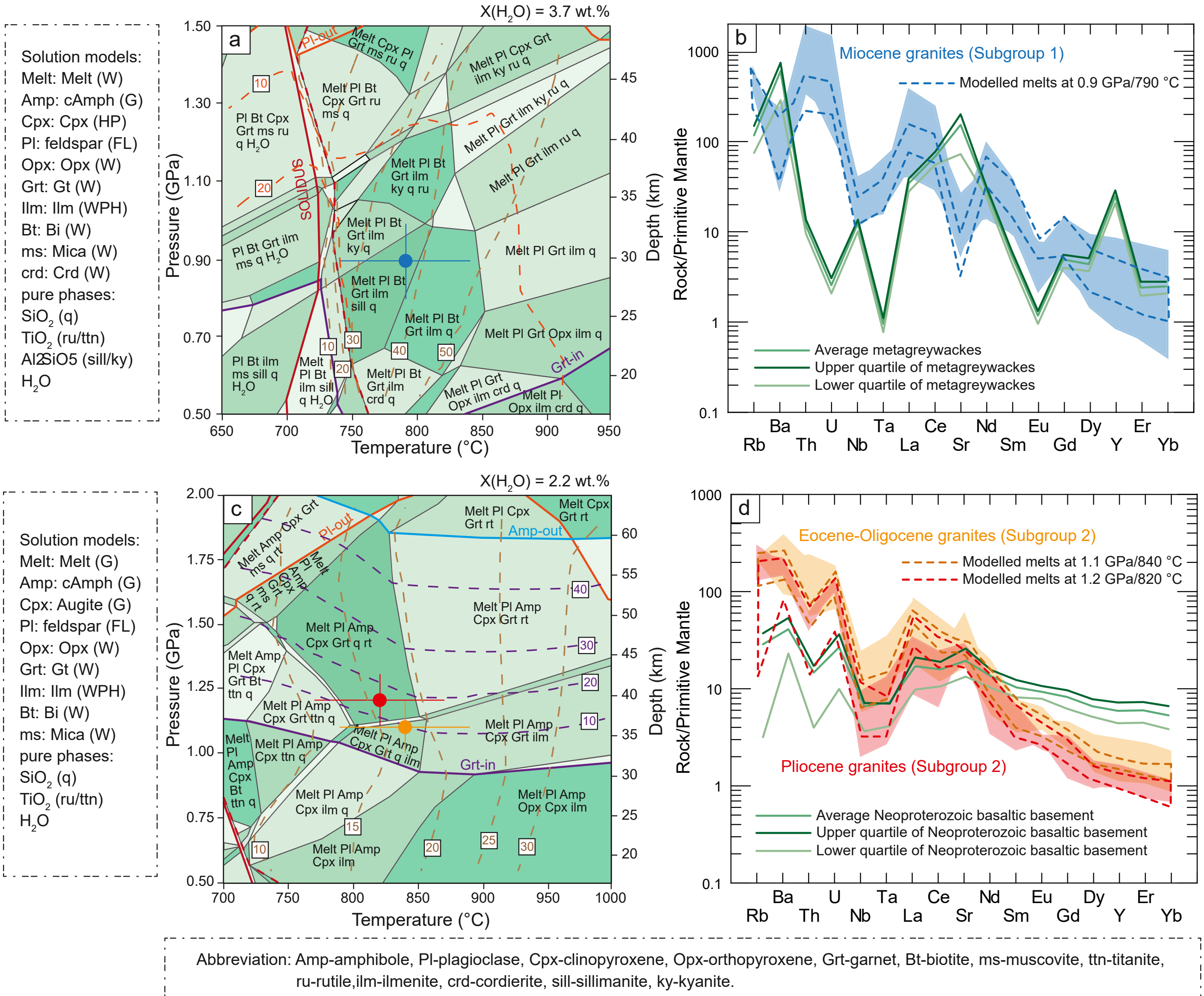

Figure 3. Thermodynamic and trace element modeling. (a, c) Simplified *P-T* phase diagram for the average composition of metasedimentary rocks from the Songpan-Ganzi Basin and Neoproterozoic mafic rocks from the western margin of the Yangtze Craton, calculated with water contents of 3.7 wt.% and 2.2 wt.%, respectively, corresponding to dehydration melting (Table S7 in Supporting Information S1). The red solid line and red dashed line mark calculated solidus and water saturation of the system, respectively. Brown dashed lines show the calculated degree of melting (wt.% of melt); purple dashed lines and orange dashed lines represent garnet and plagioclase proportion (wt.%) in the residue, respectively. Solution models: G-Green et al. (2016); FL-Fuhrman and Lindsley (1988), W/WPH-White et al. (2014), HP-Holland and Powell (2011). (b, d) Trace element patterns of granitic melts calculated at specific *P-T* conditions and the average composition of potential source rocks. The Kd used for modeling are presented in Table S9 in Supporting Information S1. The blue, pale orange, and red shaded areas represent the overall compositional range of the Subgroup 1 Miocene granites, Subgroup 2 Eocene-Oligocene granites, and Subgroup 2 Pliocene granites, respectively.

Subgroup 1 and Subgroup 2 to have involved local crustal sources in the EMTP and that those sources have remained the same throughout Mesozoic to Cenozoic time, the age range of our samples.

Thermodynamic and trace element modeling provide additional constraints on the petrogenesis of the samples. Here, we focus on the Cenozoic granites, which were emplaced during the tie frame of postulated crustal flow (Figure 3). The residual mineral assemblages, melting degrees, and major element compositions of melts were

Figure 2. Geochemical and isotopic characteristics of the Gongga-Zheduo granitic massif. (a) K_2O/Na_2O vs. SiO_2 (wt.%) diagram. (b) MgO (wt.%) vs. SiO_2 (wt.%) diagram. Fields of metabasaltic and eclogite melt, and metabasaltic and eclogite melt hybridized with peridotite are after Q. Wang et al. (2006). (c) Sr/Y vs. $(La/Yb)_N$ diagram. Subscript N denotes chondrite-normalization. (d) δEu vs. Ba/Nb diagram. $\delta Eu = Eu_N/[(Sm_N * Gd_N)$^0.5]. (e) $\varepsilon Nd(t)$ vs. $^{87}Sr/^{86}Sr(t)$ diagram. The isotopic compositions of potential source rocks were calculated at 10 Ma. (f) $\delta^{18}O$ (‰) vs. $\varepsilon Hf(t)$ diagram. The $\delta^{18}O$ (‰) values for the mantle are from Bindeman (2008). Modeling parameters are listed in Table S6 in Supporting Information S1.

obtained using the thermodynamic calculations of Connolly (2009). Trace element modeling was conducted using a simple batch melting model (Shaw, 1970). Cenozoic Subgroup 1 granites could be generated by 26%–49% melting of metasedimentary rocks at 0.8–1.0 GPa, 740°C–840°C (including uncertainty; Figure 3). Cenozoic Subgroup 2 granites could be formed by 10%–23% melting of Neoproterozoic mafic rocks at 1.0–1.3 GPa, 770°C–890°C (including uncertainty; Figure 3). Good fits were obtained for both major and trace elements, constraining their source characteristics and melting conditions (Figures 2 and 3).

4.3. Large-Scale Crustal Flow or Episodic Crustal Thickening/Uplift

Previous thermochronological studies conducted in the EMTP demonstrated a major phase of rapid uplift during the Late Miocene to Pliocene (~12–4 Ma), which was proposed to be related to large-scale crustal flow (Clark, House, et al., 2005; Schoenbohm et al., 2006; E. Wang et al., 2012; H. Zhang et al., 2016; Y.-Z. Zhang et al., 2017). In consideration of the time required for crustal thickening (~20 m.y.), the large-scale crustal flow was interpreted to have started at ~40–30 Ma (Clark, House, et al., 2005; Clark & Royden, 2000). This time is coeval to the onset of magmatism in both the NQT and EMTP (Long et al., 2015; Y.-C. Zeng et al., 2020). Previous paleo-elevation studies proposed that the NQT reached ~5,000 m elevation by the Eocene (F. Hu et al., 2020; Q. Xu et al., 2013), indicating a potential lateral pressure gradient existed. Our modeling results show that the Cenozoic magmas in the EMTP originated at ~30–40 km depth (Figure 3), similar to the depth of proposed large-scale crustal flow (Bai et al., 2010; Clark, Bush, et al., 2005; Clark & Royden, 2000).

Collectively, all the requirements for large-scale crustal flow during the Cenozoic seem to be met. However, Cenozoic granites in the EMTP have different isotopic compositions from the crustal rocks of NQT (Figure 2). If crustal flow exists, the isotopic composition of flowed materials is unlikely to be modified by local partial melts because: (a) deep-crustal derived magma is scarce in the eastern Songpan-Ganzi terrane (e.g., H. Li & Zhang, 2013); (b) melting degree of local crust should be lower than 5% (the lower limit of melt volume within the crustal flow; Bai et al., 2010; Hacker et al., 2014), which is lower than limit for melt extraction (Brown, 2013). Our data show no evidence that crustal materials derived from the NQT are found at ~30–40 km depth in the EMTP prior to the Pliocene, our youngest sample. Geophysical observations suggest that crustal flow may be occurring at present (Bai et al., 2010; Bao et al., 2015; C.-Y. Wang et al., 2010), but such young crustal flow cannot result in high elevations in the EMTP (Clark & Royden, 2000). Therefore, our results do not support long-distance crustal flow, but do not rule out regional scale (<200 km) crustal flow. The disordered and weaker crustal anisotropy in central Tibet, compared to the plateau margins, is also inconsistent with the large-scale crustal flow (Bao et al., 2020).

We interpret temporal changes in the isotopic data from Cenozoic granites in the EMTP to reflect changes to the magmatic sources during three episodes of magmatism (Figure 4).

The first magmatic episode (~50−30 Ma) is characterized by Subgroup 2 granites with depleted isotopic compositions and mantle-like δ^{18}O values (Figure 4, orange box). This episode is generally coeval with Eocene-Oligocene alkaline magmatism and carbonatites in the EMTP, that is, Mianning-Dechang (Hou et al., 2006; B. Xu et al., 2021) and Batang-Dali magmatism (Chung et al., 1998; B. Xu et al., 2021). These lithospheric mantle-derived magmas could have provided heat for locally melting of metabasaltic rocks in the middle-lower crust, which may also weaken the lithosphere. During this period, early crustal uplift has been documented in some areas in the EMTP, which is related to crustal thickening by compression (E. Wang et al., 2012; H. Zhang et al., 2016). Compressive thickening is supported by the Late Eocene to Oligocene fold and thrust in eastern Tibet (Cao et al., 2020; H. Li & Zhang, 2013) and high paleo-elevations (Hoke et al., 2014; S. Li, Currie, Rowley, & Ingalls, 2015).

The second magmatic episode (~20–10 Ma) is characterized by a shift to Subgroup 1 granites with more enriched isotope ratios and elevated δ^{18}O values (Figure 4; green box). Thermochronology data suggests this was a period of general stability with relatively slow uplift rates (E. Wang et al., 2012; H. Zhang et al., 2016; Y.-Z. Zhang et al., 2017). The isotopic data suggests that magmas from this episode involved the most supracrustal metasedimentary material with minimal mantle-involvement. In addition, the magmatism was active prior to the onset of the Xianshuihe strike-slip fault zone (~13–9 Ma; S. Wang et al., 2009; Y.-Z. Zhang et al., 2017). Hence, mantle-derived magma or shear heating are not likely the reason for this episode of magmatism. In turn, magmatism may have softened the crust and facilitated to the strike-slip movement of Xianshuihe Fault (J. Yang et al., 2020). Low exhumation rates during this time also argue against a decompression melting (E. Wang

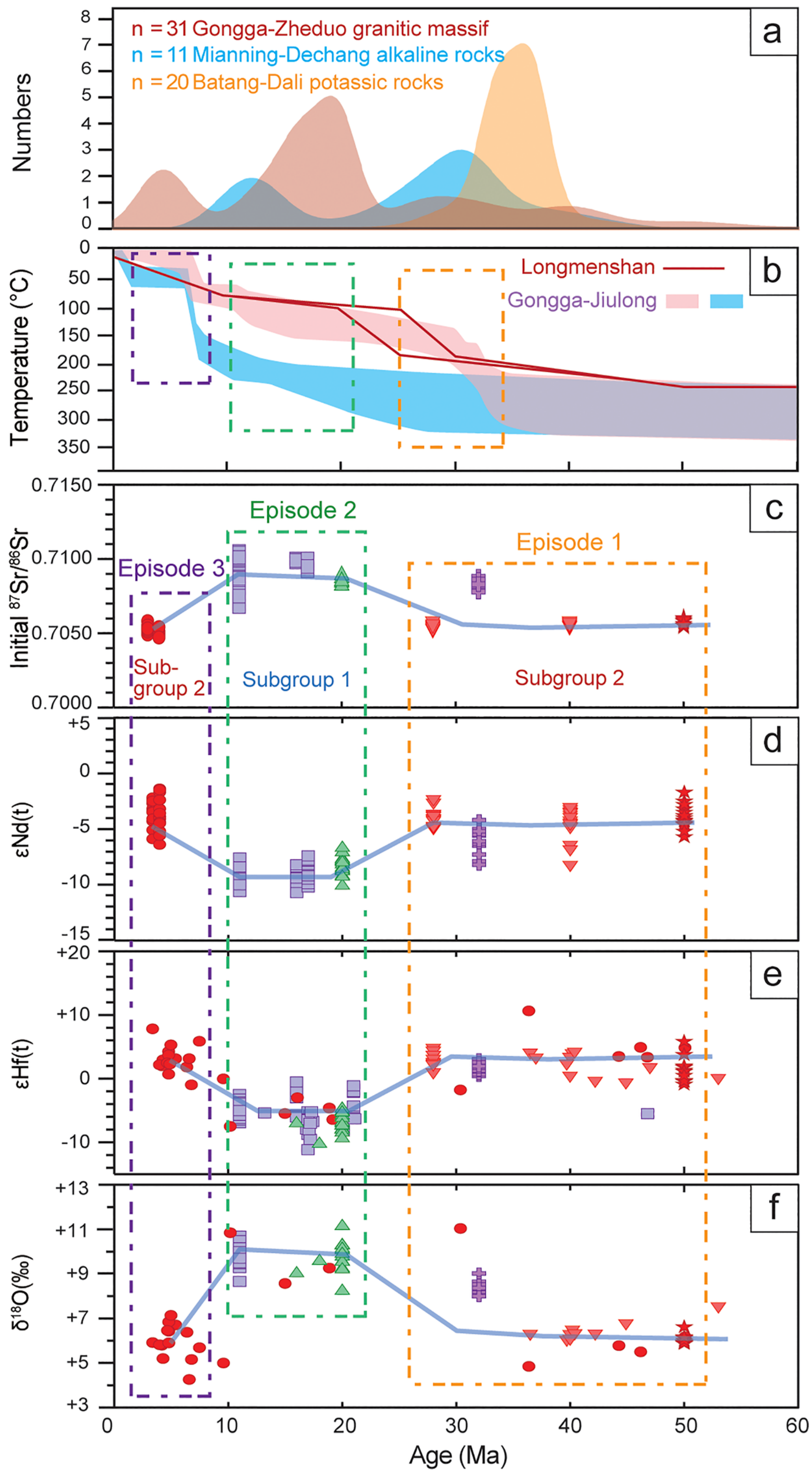

Figure 4. Temporal changes in the characteristics of Cenozoic magmatism in the EMTP. (a) Probability density plot of Gongga-Zheduo granitic massif, Mianning-Dechang alkaline rocks, and Batang-Dali alkaline rocks. Data sources are listed in Table S10 in Supporting Information S1. (b) Exhumation history of the EMTP. Data of Longmenshan and Gongga-Jiulong areas are from E. Wang et al. (2012) and H. Zhang et al. (2016), respectively. (c–f) Initial $^{87}Sr/^{86}Sr$, $\varepsilon Nd(t)$, $\varepsilon Hf(t)$, $\delta^{18}O$ (‰) vs. age (Ma) of Gongga-Zheduo granitic rocks. Three magmatic episodes, shown by orange, green and purple dashed boxes, are documented. Symbols for rock units are the same as Figure 2.

et al., 2012; H. Zhang et al., 2016). Therefore, the most likely heat source for episode 2 magmatism is radiogenic heating after crustal thickening (Bea, 2012).

The third magmatic episode (∼10–4 Ma) is characterized by Subgroup 2 granites (Figure 4, purple box), but their higher SiO_2 content, Rb/Sr, and Th/La ratios with lower La content reflect higher degrees of fractionation than granites of episode 1 (Figure S7 in Supporting Information S1). The EMTP was experiencing uplift and exhumation during this time (Clark, House, et al., 2005; E. Wang et al., 2012; H. Zhang et al., 2016). There are several lines of evidence to suggest that this is related to upwelling of asthenospheric mantle including (a) ∼12 Ma alkaline rocks in the Mianning-Dechang area (B. Xu et al., 2021), (b) abnormally high lithospheric heat flow, mantle signatures of $^3He/^4He$ from hot springs (S. Hu et al., 2000; M. Zhang et al., 2021), (c) upper mantle low-velocity anomalies (Z. Huang et al., 2019; W. Wang et al., 2021), and (d) dynamic support for high elevations (Bao et al., 2020). Geophysical observations suggest that northwestward downwelling of the Indian Block (Z. Huang et al., 2019) and regional lithospheric delamination (W. Wang et al., 2021) could account for the upwelling of the asthenosphere. We suggest that mantle upwelling caused (re)melting of metabasaltic rocks in the EMTP during episode 3.

5. Conclusions

The Gongga-Zheduo granitic massif contains Mesozoic (∼214–172 Ma) to Cenozoic (∼50–4 Ma) granitoid rocks and helps to constrain crustal compositions and sources in the EMTP. The granitoid rocks can be divided into two subgroups according to their geochemical and isotopic characteristics. Subgroup 1 was derived from partial melting of metasedimentary rocks of Songpan-Ganzi terrane, and Subgroup 2 was derived from partial melting of metabasaltic rocks of western margin of the Yangtze Craton. Evidence for crustal materials derived from the NQT were not observed and we suggest that the mid-lower crust in the EMTP consists entirely of locally derived crustal rocks. Changes in the magmatic sources during the Cenozoic correlate well with changes in uplift and exhumation. Cenozoic magmatism was primarily controlled by mantle-crust interactions, which in turn may have modified the lithospheric (especially crustal) rheology in eastern Tibet. The continued indentation of India and changes in crustal rheology of Asia shaped the present eastern boundary of the Tibetan Plateau.

Data Availability Statement

All the data for this research are available in Supporting Information S1 and online (https://doi.org/10.6084/m9.figshare.19376033.v2).

Acknowledgments
F. Y. H. and F. Y. W. acknowledge support from National Natural Science Foundation of China (41888101 and 41902055) and China Postdoctoral Science Foundation (2018M640177). M. N. D. acknowledges support from U.S. National Science Foundation (EAR-1725002) and the Romanian Executive Agency for Higher Education, Research, Development and Innovation Funding project (PN-III-P4-ID-PCCF-2016-0014). Yalu Hu and Guozheng Sun are thanked for help in thermodynamic modeling. Guohui Chen and Yulu Tian are thanked for help in field. The authors declare no conflict of interest. The authors thank two anonymous reviewers and Editor Lucy Flesch for their constructive comments.

References

Bai, D., Unsworth, M. J., Meju, M. A., Ma, X., Teng, J., Kong, X., et al. (2010). Crustal deformation of the eastern Tibetan Plateau revealed by magnetotelluric imaging. *Nature Geoscience*, *3*(5), 358–362. https://doi.org/10.1038/ngeo830

Bao, X., Song, X., Eaton, D. W., Xu, Y., & Chen, H. (2020). Episodic lithospheric deformation in eastern Tibet inferred from seismic anisotropy. *Geophysical Research Letters*, *47*(3), e2019GL085721. https://doi.org/10.1029/2019GL085721

Bao, X., Sun, X., Xu, M., Eaton, D. W., Song, X., Wang, L., et al. (2015). Two crustal low-velocity channels beneath SE Tibet revealed by joint inversion of Rayleigh wave dispersion and receiver functions. *Earth and Planetary Science Letters*, *415*, 16–24. https://doi.org/10.1016/j.epsl.2015.01.020

Bea, F. (2012). The sources of energy for crustal melting and the geochemistry of heat-producing elements. *Lithos*, *153*, 278–291. https://doi.org/10.1016/j.lithos.2012.01.017

Bindeman, I. (2008). Oxygen isotopes in mantle and crustal magmas as revealed by single crystal analysis. *Reviews in Mineralogy and Geochemistry*, *69*(1), 445–478. https://doi.org/10.2138/rmg.2008.69.12

Brown, M. (2013). Granite: From genesis to emplacement. *GSA Bulletin*, *125*(7–8), 1079–1113. https://doi.org/10.1130/B30877.1

Cao, K., Leloup, P. H., Wang, G., Liu, W., Mahéo, G., Shen, T., et al. (2020). Thrusting, exhumation, and basin fill on the western margin of the south China block during the India-Asia collision. *GSA Bulletin*, *133*(1–2), 74–90. https://doi.org/10.1130/B35349.1

Castillo, P. R. (2012). Adakite petrogenesis. *Lithos*, *134–135*, 304–316. https://doi.org/10.1016/j.lithos.2011.09.013

Chen, Q., Sun, M., Zhao, G., Yang, F., Long, X., Li, J., et al. (2017). Origin of the mafic microgranular enclaves (MMEs) and their host granitoids from the Tagong pluton in Songpan-Ganze terrane: An igneous response to the closure of the Paleo-Tethys ocean. *Lithos*, *290–291*, 1–17. https://doi.org/10.1016/j.lithos.2017.07.019

Chen, Y., Zhang, G., Lu, R., Luo, T., Li, Y., & Yu, W. (2020). Formation and evolution of Xianshuihe Fault Belt in the eastern margin of the Tibetan Plateau: Constraints from structural deformation and geochronology. *Geological Journal*, *55*(12), 7953–7976. https://doi.org/10.1002/gj.3908

Chung, S.-L., Chu, M.-F., Zhang, Y., Xie, Y., Lo, C.-H., Lee, T.-Y., et al. (2005). Tibetan tectonic evolution inferred from spatial and temporal variations in post-collisional magmatism. *Earth-Science Reviews*, *68*(3–4), 173–196. https://doi.org/10.1016/j.earscirev.2004.05.001

Chung, S.-L., Lo, C.-H., Lee, T.-Y., Zhang, Y., Xie, Y., Li, X., et al. (1998). Diachronous uplift of the Tibetan Plateau starting 40 Myr ago. *Nature*, *394*(6695), 769–773. https://doi.org/10.1038/29511

Clark, M. K., Bush, J. W. M., & Royden, L. H. (2005). Dynamic topography produced by lower crustal flow against rheological strength heterogeneities bordering the Tibetan Plateau. *Geophysical Journal International*, *162*(2), 575–590. https://doi.org/10.1111/j.1365-246X.2005.02580.x

Clark, M. K., House, M. A., Royden, L. H., Whipple, K. X., Burchfiel, B. C., Zhang, X., & Tang, W. (2005). Late Cenozoic uplift of southeastern Tibet. *Geology*, *33*(6), 525–528. https://doi.org/10.1130/G21265.1

Clark, M. K., & Royden, L. H. (2000). Topographic ooze: Building the eastern margin of Tibet by lower crustal flow. *Geology*, *28*(8). https://doi.org/10.1130/0091-7613(2000)28<703:tobtem>2.0.co;2

Connolly, J. a. D. (2009). The geodynamic equation of state: What and how. *Geochemistry, Geophysics, Geosystems*, *10*(10). https://doi.org/10.1029/2009GC002540

de Sigoyer, J., Vanderhaeghe, O., Duchêne, S., & Billerot, A. (2014). Generation and emplacement of Triassic granitoids within the Songpan Ganze accretionary-orogenic wedge in a context of slab retreat accommodated by tear faulting, eastern Tibetan Plateau, China. *Journal of Asian Earth Sciences*, *88*, 192–216. https://doi.org/10.1016/j.jseaes.2014.01.010

England, P., & Houseman, G. (1986). Finite strain calculations of continental deformation: 2. Comparison with the India-Asia collision zone. *Journal of Geophysical Research: Solid Earth*, *91*(B3), 3664–3676. https://doi.org/10.1029/JB091iB03p03664

England, P., & Molnar, P. (1997). Active deformation of Asia: From kinematics to dynamics. *Science*, *278*, 647–650. https://doi.org/10.1126/science.278.5338.647

Forshaw, J. B., & Pattison, D. R. M. (2021). Ferrous/ferric (Fe^{2+}/Fe^{3+}) partitioning among silicates in metapelites. *Contributions to Mineralogy and Petrology*, *176*(9), 63. https://doi.org/10.1007/s00410-021-01814-4

Hacker, B. R., Ritzwoller, M. H., & Xie, J. (2014). Partially melted, mica-bearing crust in Central Tibet. *Tectonics*, *33*(7), 1408–1424. https://doi.org/10.1002/2014TC003545

Hoke, G. D., Liu-Zeng, J., Hren, M. T., Wissink, G. K., & Garzione, C. N. (2014). Stable isotopes reveal high southeast Tibetan Plateau margin since the Paleogene. *Earth and Planetary Science Letters*, *394*, 270–278. https://doi.org/10.1016/j.epsl.2014.03.007

Hou, Z., Tian, S., Yuan, Z., Xie, Y., Yin, S., Yi, L., et al. (2006). The Himalayan collision zone carbonatites in western Sichuan, SW China: Petrogenesis, mantle source, and tectonic implication. *Earth and Planetary Science Letters*, *244*(1–2), 234–250. https://doi.org/10.1016/j.epsl.2006.01.052

Huang, Z., Wang, L., Xu, M., Zhao, D., Mi, N., & Yu, D. (2019). *P* and *S* wave tomography beneath the SE Tibetan Plateau: Evidence for lithospheric delamination. *Journal of Geophysical Research: Solid Earth*, *124*(10), 10292–10308. https://doi.org/10.1029/2019JB017430

King, J., Harris, N., Argles, T., Parrish, R., Charlier, B., Sherlock, S., & Zhang, H. F. (2007). First field evidence of southward ductile flow of Asian crust beneath southern Tibet. *Geology*, *35*(8), 727–730. https://doi.org/10.1130/G23630A.1

Kong, F., Wu, J., Liu, K. H., & Gao, S. S. (2016). Crustal anisotropy and ductile flow beneath the eastern Tibetan Plateau and adjacent areas. *Earth and Planetary Science Letters*, *442*, 72–79. https://doi.org/10.1016/j.epsl.2016.03.003

Kruse, S., McNutt, M., Phipps-Morgan, J., Royden, L., & Wernicke, B. (1991). Lithospheric extension near Lake Mead, Nevada: A model for ductile flow in the lower crust. *Journal of Geophysical Research: Solid Earth*, *96*(B3), 4435–4456. https://doi.org/10.1029/90JB02621

Lai, S., & Zhao, S. (2018). Petrogenesis of the Zheduoshan Cenozoic granites in the eastern margin of Tibet: Constraints on the initial activity of the Xianshuihe fault. *Journal of Geodynamics*, *117*, 49–59. https://doi.org/10.1016/j.jog.2018.03.009

Li, H., & Zhang, Y. (2013). Zircon U-Pb geochronology of the Konggar granitoid and migmatite: Constraints on the Oligo-Miocene tectono-thermal evolution of the Xianshuihe fault zone, East Tibet. *Tectonophysics*, *606*, 127–139. https://doi.org/10.1016/j.tecto.2013.07.007

Li, H., Zhang, Y., Zhang, C., Dong, S., & Zhu, F. (2015). Middle Jurassic syn-kinematic magmatism, anatexis, and metamorphism in the Zheduo-Gonggar massif, implication for the deformation of the Xianshuihe fault zone, East Tibet. *Journal of Asian Earth Sciences*, *107*, 35–52. https://doi.org/10.1016/j.jseaes.2015.03.038

Li, H., Zhang, Y., Zhang, C., & Wang, J. (2016). Zircon U-Pb study of two-staged Oligo-Miocene migmatization along the Xianshuihe fault zone, East Tibet Plateau. *Earth Science Frontiers*, *23*(2), 222–237. (in Chinese with English abstract).

Li, S., Currie, B. S., Rowley, D. B., & Ingalls, M. (2015). Cenozoic paleoaltimetry of the SE margin of the Tibetan Plateau: Constraints on the tectonic evolution of the region. *Earth and Planetary Science Letters*, *432*, 415–424. https://doi.org/10.1016/j.epsl.2015.09.044

Li, S., Miller, C. F., Tao, W., Xiao, W., & Chew, D. (2021). Role of sediment in generating contemporaneous, diverse "type" granitoid magmas. *Geology*, *50*(4), 427–431. https://doi.org/10.1130/G49509.1

Liu, Q. Y., van der Hilst, R. D., Li, Y., Yao, H. J., Chen, J. H., Guo, B., et al. (2014). Eastward expansion of the Tibetan Plateau by crustal flow and strain partitioning across faults. *Nature Geoscience*, *7*(5), 361–365. https://doi.org/10.1038/ngeo2130

Long, X., Wilde, S. A., Wang, Q., Yuan, C., Wang, X.-C., Li, J., et al. (2015). Partial melting of thickened continental crust in central Tibet: Evidence from geochemistry and geochronology of Eocene adakitic rhyolites in the northern Qiangtang Terrane. *Earth and Planetary Science Letters*, *414*, 30–44. https://doi.org/10.1016/j.epsl.2015.01.007

MacCready, T., Snoke, A. W., Wright, J. E., & Howard, K. A. (1997). Mid-crustal flow during Tertiary extension in the Ruby Mountains core complex, Nevada. *GSA Bulletin*, *109*(12), 1576–1594. https://doi.org/10.1130/0016-7606(1997)109<1576:mcfdte>2.3.co;2;2

Mayne, M. J., Moyen, J.-F., Stevens, G., & Kaislaniemi, L. (2016). Rcrust: A tool for calculating path-dependent open system processes and application to melt loss. *Journal of Metamorphic Geology*, *34*(7), 663–682. https://doi.org/10.1111/jmg.12199

McKenzie, D., Nimmo, F., Jackson, J. A., Gans, P. B., & Miller, E. L. (2000). Characteristics and consequences of flow in the lower crust. *Journal of Geophysical Research: Solid Earth*, *105*(B5), 11029–11046. https://doi.org/10.1029/1999JB900446

Molnar, P., & Tapponnier, P. (1975). Cenozoic tectonics of Asia: Effects of a continental collision. *Features of Recent Continental Tectonics in Asia Can Be Interpreted as Results of the India-Eurasia Collision*, *189*(4201), 419–426. https://doi.org/10.1126/science.189.4201.419

Moyen, J.-F. (2009). High Sr/Y and La/Yb ratios: The meaning of the "adakitic signature". *Lithos*, *112*(3–4), 556–574. https://doi.org/10.1016/j.lithos.2009.04.001

Palin, R. M., Weller, O. M., Waters, D. J., & Dyck, B. (2016). Quantifying geological uncertainty in metamorphic phase equilibria modeling; a Monte Carlo assessment and implications for tectonic interpretations. *Geoscience Frontiers*, *7*(4), 591–607. https://doi.org/10.1016/j.gsf.2015.08.005

Patiño Douce, A. E. (1999). What do experiments tell us about the relative contributions of crust and mantle to the origin of granitic magmas? *Geological Society, London, Special Publications*, *168*(1), 55–75. https://doi.org/10.1144/gsl.sp.1999.168.01.05

Peng, T., Zhao, G., Fan, W., Peng, B., & Mao, Y. (2015). Late Triassic granitic magmatism in the eastern Qiangtang, eastern Tibetan Plateau: Geochronology, petrogenesis and implications for the tectonic evolution of the Paleo-Tethys. *Gondwana Research*, *27*(4), 1494–1508. https://doi.org/10.1016/j.gr.2014.01.009

Pourteau, A., Doucet, L. S., Blereau, E. R., Volante, S., Johnson, T. E., Collins, W. J., et al. (2020). TTG generation by fluid-fluxed crustal melting: Direct evidence from the Proterozoic Georgetown Inlier, NE Australia. *Earth and Planetary Science Letters*, *550*, 116548. https://doi.org/10.1016/j.epsl.2020.116548

Roger, F., Calassou, S., Lancelot, J., Malavieille, J., Mattauer, M., Zhiqin, X., et al. (1995). Miocene emplacement and deformation of the Konga Shan granite (Xianshui He fault zone, west Sichuan, China): Geodynamic implications. *Earth and Planetary Science Letters*, *130*(1), 201–216. https://doi.org/10.1016/0012-821X(94)00252-T

Royden, L. H., Burchfiel, B. C., King, R. W., Wang, E., Chen, Z. L., Shen, F., & Liu, Y. (1997). Surface deformation and lower crustal flow in eastern Tibet. *Science*, *276*, 788–790. https://doi.org/10.1126/science.276.5313.788

Schoenbohm, L. M., Burchfiel, B. C., & Liangzhong, C. (2006). Propagation of surface uplift, lower crustal flow, and Cenozoic tectonics of the southeast margin of the Tibetan Plateau. *Geology*, *34*(10). https://doi.org/10.1130/g22679.1

Searle, M. P., Roberts, N. M. W., Chung, S.-L., Lee, Y.-H., Cook, K. L., Elliott, J. R., et al. (2016). Age and anatomy of the Gongga Shan batholith, eastern Tibetan Plateau, and its relationship to the active Xianshui-he fault. *Geosphere*, *12*(3), 948–970. https://doi.org/10.1130/ges01244.1

Shaw, D. M. (1970). Trace element fractionation during anatexis. *Geochimica et Cosmochimica Acta*, *34*(2), 237–243. https://doi.org/10.1016/0016-7037(70)90009-8

Song, S.-W., Zhu, D.-C., Wang, Q., Cawood, P. A., Zhan, Q.-Y., Li, S.-M., et al. (2021). Generation of syn-collisional S-type granites in collision zones: An example from the Late Triassic Tanggula Batholith in northern Tibet. *Gondwana Research*, *104*, 185–198. https://doi.org/10.1016/j.gr.2020.12.023

Sun, S.-s., & McDonough, W. F. (1989). Chemical and isotopic systematics of oceanic basalts: Implications for mantle composition and processes. *Geological Society, London, Special Publications*, *42*(1), 313. https://doi.org/10.1144/GSL.SP.1989.042.01.19

Tapponnier, P., Zhiqin, X., Roger, F., Meyer, B., Arnaud, N., Wittlinger, G., & Jingsui, Y. (2001). Oblique stepwise rise and growth of the Tibet Plateau. *Science*, *294*(5547), 1671–1677. https://doi.org/10.1126/science.105978

Wang, C.-Y., Lou, H., Silver, P. G., Zhu, L., & Chang, L. (2010). Crustal structure variation along 30°N in the eastern Tibetan Plateau and its tectonic implications. *Earth and Planetary Science Letters*, *289*(3–4), 367–376. https://doi.org/10.1016/j.epsl.2009.11.026

Wang, E., Kirby, E., Furlong, K. P., van Soest, M., Xu, G., Shi, X., et al. (2012). Two-phase growth of high topography in eastern Tibet during the Cenozoic. *Nature Geoscience*, *5*(9), 640–645. https://doi.org/10.1038/ngeo1538

Wang, Q., Hawkesworth, C. J., Wyman, D., Chung, S.-L., Wu, F.-Y., Li, X.-H., et al. (2016). Pliocene-Quaternary crustal melting in central and northern Tibet and insights into crustal flow. *Nature Communications*, *7*, 11888. https://doi.org/10.1038/ncomms11888

Wang, Q., Xu, J.-F., Jian, P., Bao, Z.-W., Zhao, Z.-H., Li, C.-F., et al. (2006). Petrogenesis of adakitic porphyries in an extensional tectonic setting, Dexing, south China: Implications for the genesis of porphyry copper mineralization. *Journal of Petrology*, *47*(1), 119–144. https://doi.org/10.1093/petrology/egi070

Wang, S., Fang, X., Zheng, D., & Wang, E. (2009). Initiation of slip along the Xianshuihe fault zone, eastern Tibet, constrained by K/Ar and fission-track ages. *International Geology Review*, *51*(12), 1121–1131. https://doi.org/10.1080/00206810902945132

Wang, W., Wu, J., & Hammond, J. O. S. (2021). Mantle dynamics beneath the Sichuan Basin and eastern Tibet from teleseismic tomography. *Tectonics*, *40*(2). https://doi.org/10.1029/2020TC006319

Whittington, A. G., Hofmeister, A. M., & Nabelek, P. I. (2009). Temperature-dependent thermal diffusivity of the Earth's crust and implications for magmatism. *Nature*, *458*(7236), 319–321. https://doi.org/10.1038/nature07818

Xu, B., Hou, Z.-Q., Griffin, W. L., Zheng, Y.-C., Wang, T., Guo, Z., et al. (2021). Cenozoic lithospheric architecture and metallogenesis in Southeastern Tibet. *Earth-Science Reviews*, *214*, 103472. https://doi.org/10.1016/j.earscirev.2020.103472

Xu, Q., Ding, L., Zhang, L., Cai, F., Lai, Q., Yang, D., & Liu-Zeng, J. (2013). Paleogene high elevations in the Qiangtang Terrane, central Tibetan Plateau. *Earth and Planetary Science Letters*, *362*, 31–42. https://doi.org/10.1016/j.epsl.2012.11.058

Yang, J., Kaus, B. J. P., Li, Y., Leloup, P. H., Popov, A. A., Lu, G., et al. (2020). Lower crustal rheology controls the development of large offset strike-slip faults during the Himalayan-Tibetan orogeny. *Geophysical Research Letters*, *47*(18), e2020GL089435. https://doi.org/10.1029/2020GL089435

Yang, J.-H., Wu, F.-Y., Wilde, S. A., Xie, L.-W., Yang, Y.-H., & Liu, X.-M. (2007). Tracing magma mixing in granite genesis: In situ U-Pb dating and Hf-isotope analysis of zircons. *Contributions to Mineralogy and Petrology*, *153*(2), 177–190. https://doi.org/10.1007/s00410-006-0139-7

Zeng, L., Gao, L.-E., Xie, K., & Liu-Zeng, J. (2011). Mid-Eocene high Sr/Y granites in the Northern Himalayan gneiss domes: Melting thickened lower continental crust. *Earth and Planetary Science Letters*, *303*(3), 251–266. https://doi.org/10.1016/j.epsl.2011.01.005

Zeng, Y.-C., Ducea, M. N., Xu, J., Chen, J., & Dong, Y.-H. (2020). Negligible surface uplift following foundering of thickened central Tibetan lower crust. *Geology*, *49*(1), 45–50. https://doi.org/10.1130/G48142.1

Zhang, H., Oskin, M. E., Liu-Zeng, J., Zhang, P., Reiners, P. W., & Xiao, P. (2016). Pulsed exhumation of interior eastern Tibet: Implications for relief generation mechanisms and the origin of high-elevation planation surfaces. *Earth and Planetary Science Letters*, *449*, 176–185. https://doi.org/10.1016/j.epsl.2016.05.048

Zhang, M., Guo, Z., Xu, S., Barry, P. H., Sano, Y., Zhang, L., et al. (2021). Linking deeply-sourced volatile emissions to plateau growth dynamics in southeastern Tibetan Plateau. *Nature Communications*, *12*(1), 4157. https://doi.org/10.1038/s41467-021-24415-y

Zhang, Y.-Z., Replumaz, A., Leloup, P. H., Wang, G.-C., Bernet, M., van der Beek, P., et al. (2017). Cooling history of the Gongga batholith: Implications for the Xianshuihe fault and Miocene kinematics of SE Tibet. *Earth and Planetary Science Letters*, *465*, 1–15. https://doi.org/10.1016/j.epsl.2017.02.025

Zhao, J.-H., Li, Q.-W., Liu, H., & Wang, W. (2018). Neoproterozoic magmatism in the western and northern margins of the Yangtze Block (south China) controlled by slab subduction and subduction-transform-edge-propagator. *Earth-Science Reviews*, *187*, 1–18. https://doi.org/10.1016/j.earscirev.2018.10.004

Zhou, Z., & Lei, J. (2016). Pn anisotropic tomography and mantle dynamics beneath China. *Physics of the Earth and Planetary Interiors*, *257*, 193–204. https://doi.org/10.1016/j.pepi.2016.06.005

References From the Supporting Information

Bédard, J. H. (2006). A catalytic delamination-driven model for coupled genesis of Archaean crust and sub-continental lithospheric mantle. *Geochimica et Cosmochimica Acta*, *70*(5), 1188–1214. https://doi.org/10.1016/j.gca.2005.11.008

Blichert-Toft, J., & Albarède, F. (1997). The Lu-Hf isotope geochemistry of chondrites and the evolution of the mantle-crust system. *Earth and Planetary Science Letters*, *148*(1), 243–258. https://doi.org/10.1016/S0012-821X(97)00040-X

DePaolo, D. J. (1981). Trace element and isotopic effects of combined wallrock assimilation and fractional crystallization. *Earth and Planetary Science Letters*, *53*(2), 189–202. https://doi.org/10.1016/0012-821X(81)90153-9

Fei, G., Menuge, J. F., Li, Y., Yang, J., Deng, Y., Chen, C., et al. (2020). Petrogenesis of the Lijiagou spodumene pegmatites in Songpan-Garze Fold Belt, west Sichuan, China: Evidence from geochemistry, zircon, cassiterite and coltan U-Pb geochronology and Hf isotopic compositions. *Lithos*, *364–365*, 105555. https://doi.org/10.1016/j.lithos.2020.105555

Fuhrman, M. L., & Lindsley, D. H. (1988). Ternary-feldspar modeling and thermometry. *American Mineralogist*, *73*(3–4), 201–215.

Green, E. C. R., White, R. W., Diener, J. F. A., Powell, R., Holland, T. J. B., & Palin, R. M. (2016). Activity-composition relations for the calculation of partial melting equilibria in metabasic rocks. *Journal of Metamorphic Geology*, *34*(9), 845–869. https://doi.org/10.1111/jmg.12211

Griffin, W. L., Pearson, N. J., Belousova, E., Jackson, S. E., van Achterbergh, E., O'Reilly, S. Y., & Shee, S. R. (2000). The Hf isotope composition of cratonic mantle: LAM-MC-ICPMS analysis of zircon megacrysts in kimberlites. *Geochimica et Cosmochimica Acta*, *64*(1), 133–147. https://doi.org/10.1016/S0016-7037(99)00343-9

Holland, T. J. B., & Powell, R. (2011). An improved and extended internally consistent thermodynamic dataset for phases of petrological interest, involving a new equation of state for solids. *Journal of Metamorphic Geology*, *29*(3), 333–383. https://doi.org/10.1111/j.1525-1314.2010.00923.x

Hu, F., Wu, F., Chapman, J. B., Ducea, M. N., Ji, W., & Liu, S. (2020). Quantitatively tracking the elevation of the Tibetan Plateau since the Cretaceous: Insights from whole-rock Sr/Y and La/Yb ratios. *Geophysical Research Letters*, *47*(15), e2020GL089202. https://doi.org/10.1029/2020GL089202

Hu, S., He, L., & Wang, J. (2000). Heat flow in the continental area of China: A new data set. *Earth and Planetary Science Letters*, *179*(2), 407–419. https://doi.org/10.1016/S0012-821X(00)00126-6

Huang, C., Wang, H., Yang, J.-H., Ramezani, J., Yang, C., Zhang, S.-B., et al. (2020). SA01—A proposed zircon reference material for microbeam U-Pb age and Hf-O isotopic determination. *Geostandards and Geoanalytical Research*, *44*(1), 103–123. https://doi.org/10.1111/ggr.12307

Jackson, S. E., Pearson, N. J., Griffin, W. L., & Belousova, E. A. (2004). The application of laser ablation-inductively coupled plasma-mass spectrometry to in situ U-Pb zircon geochronology. *Chemical Geology*, *211*(1), 47–69. https://doi.org/10.1016/j.chemgeo.2004.06.017

Li, Q.-L., Li, X.-H., Liu, Y., Tang, G.-Q., Yang, J.-H., & Zhu, W.-G. (2010). Precise U-Pb and Pb-Pb dating of Phanerozoic baddeleyite by SIMS with oxygen flooding technique. *Journal of Analytical Atomic Spectrometry*, *25*(7), 1107–1113. https://doi.org/10.1039/B923444F

Li, X.-H., Liu, Y., Li, Q.-L., Guo, C.-H., & Chamberlain, K. R. (2009). Precise determination of Phanerozoic zircon Pb/Pb age by multicollector SIMS without external standardization. *Geochemistry, Geophysics, Geosystems*, *10*(4). https://doi.org/10.1029/2009GC002400

Li, X.-H., Long, W.-G., Li, Q.-L., Liu, Y., Zheng, Y.-F., Yang, Y.-H., et al. (2010). Penglai zircon megacrysts: A potential new working reference material for microbeam determination of Hf-O isotopes and U-Pb age. *Geostandards and Geoanalytical Research*, *34*(2), 117–134. https://doi.org/10.1111/j.1751-908X.2010.00036.x

Li, X.-H., Tang, G., Gong, B., Yang, Y., Hou, K., Hu, Z., et al. (2013). Qinghu zircon: A working reference for microbeam analysis of U-Pb age and Hf and O isotopes. *Chinese Science Bulletin*, *58*(36), 4647–4654. https://doi.org/10.1007/s11434-013-5932-x

Liu, S., Wang, Z., Yan, Q., Li, Q., Zhang, D., & Wang, J. (2006). Timing, petrogenesis and geodynamic significance of Zheduoshan Granitoids. *Acta Petrologica Sinica*, *22*(2), 343–352. (in Chinese with English abstract).

Liu, Y., Zhu, Z., Chen, C., Zhang, S., Sun, X., Yang, Z., & Liang, W. (2015). Geochemical and mineralogical characteristics of weathered ore in the Dalucao REE deposit, Mianning-Dechang REE Belt, western Sichuan Province, southwestern China. *Ore Geology Reviews*, *71*, 437–456. https://doi.org/10.1016/j.oregeorev.2015.06.009

Lu, L., Zhang, K.-J., Yan, L.-L., Jin, X., & Zhang, Y.-X. (2017). Was Late Triassic Tanggula granitoid (central Tibet, western China) a product of melting of underthrust Songpan-Ganzi flysch sediments? *Tectonics*, *36*(5), 902–928. https://doi.org/10.1002/2016tc004384

Ludwig, K. R. (2012). *A geochronological toolkit for Microsoft Excel* (Vol. 5). Berkeley Geochronology Center, Special Publication.

Maniar, P. D., & Piccoli, P. M. (1989). Tectonic discrimination of granitoids. *The Geological Society of America Bulletin*, *101*(5), 635–643.

Middlemost, E. A. K. (1994). Naming materials in the magma/igneous rock system. *Earth-Science Reviews*, *37*(3–4), 215–224. https://doi.org/10.1016/0012-8252(94)90029-9

Montel, J.-M., & Vielzeuf, D. (1997). Partial melting of metagreywackes, part II. Compositions of minerals and melts. *Contributions to Mineralogy and Petrology*, *128*(2), 176–196. https://doi.org/10.1007/s004100050302

Nandedkar, R. H., Hürlimann, N., Ulmer, P., & Müntener, O. (2016). Amphibole-melt trace element partitioning of fractionating calc-alkaline magmas in the lower crust: An experimental study. *Contributions to Mineralogy and Petrology*, *171*(8), 71. https://doi.org/10.1007/s00410-016-1278-0

Nash, W. P., & Crecraft, H. R. (1985). Partition coefficients for trace elements in silicic magmas. *Geochimica et Cosmochimica Acta*, *49*(11), 2309–2322. https://doi.org/10.1016/0016-7037(85)90231-5

Patiño Douce, A. E., & Harris, N. (1998). Experimental constraints on Himalayan anatexis. *Journal of Petrology*, *39*(4), 689–710.

Qian, Q., & Hermann, J. (2013). Partial melting of lower crust at 10–15 kbar: Constraints on adakite and TTG formation. *Contributions to Mineralogy and Petrology*, *165*(6), 1195–1224. https://doi.org/10.1007/s00410-013-0854-9

Rapp, R. P., Shimizu, N., Norman, M. D., & Applegate, G. S. (1999). Reaction between slab-derived melts and peridotite in the mantle wedge: Experimental constraints at 3.8 GPa. *Chemical Geology*, *160*(4), 335–356.

Rapp, R. P., & Watson, E. B. (1995). Dehydration melting of metabasalt at 8–32 kbar: Implications for continental growth and crust-mantle recycling. *Journal of Petrology*, *36*(4), 891–931. https://doi.org/10.1093/petrology/36.4.891

Rollinson, H. R. (1993). *Using geochemical data: Evaluation, presentation, interpretation*. Longman Scientific & Technical.

She, Z., Ma, C., Mason, R., Li, J., Wang, G., & Lei, Y. (2006). Provenance of the Triassic Songpan-Ganzi flysch, west China. *Chemical Geology*, *231*(1), 159–175. https://doi.org/10.1016/j.chemgeo.2006.01.001

Sisson, T. W., Ratajeski, K., Hankins, W. B., & Glazner, A. F. (2005). Voluminous granitic magmas from common basaltic sources. *Contributions to Mineralogy and Petrology*, *148*(6), 635–661. https://doi.org/10.1007/s00410-004-0632-9

Smithies, R. H. (2000). The Archaean tonalite-trondhjemite-granodiorite (TTG) series is not an analog of Cenozoic adakite. *Earth and Planetary Science Letters*, *182*(1), 115–125. https://doi.org/10.1016/S0012-821X(00)00236-3

Stacey, J. S., & Kramers, J. D. (1975). Approximation of terrestrial lead isotope evolution by a two-stage model. *Earth and Planetary Science Letters*, *26*(2), 207–221. https://doi.org/10.1016/0012-821X(75)90088-6

Stern, C. R., & Kilian, R. (1996). Role of the subducted slab, mantle wedge and continental crust in the generation of adakites from the Andean Austral Volcanic Zone. *Contributions to Mineralogy and Petrology*, *123*(3), 263–281.

Valley, J. W., Kinny, P. D., Schulze, D. J., & Spicuzza, M. J. (1998). Zircon megacrysts from kimberlite: Oxygen isotope variability among mantle melts. *Contributions to Mineralogy and Petrology*, *133*(1), 1–11. https://doi.org/10.1007/s004100050432

van Achterbergh, E., Ryan, C., Jackson, S., & Griffin, W. L. (2001). Appendix 3 data reduction software for LA-ICP-MS. In P. Sylvester (Ed.), *Laser-ablation-ICPMS in the Earth Sciences* (pp. 239–243). Quebec, Canada: Mineralogical Association of Canada Short Course.

White, R. W., Powell, R., & Johnson, T. E. (2014). The effect of Mn on mineral stability in metapelites revisited: New *a-x* relations for manganese-bearing minerals. *Journal of Metamorphic Geology*, *32*(8), 809–828. https://doi.org/10.1111/jmg.12095

Wiedenbeck, M., AllÉ, P., Corfu, F., Griffin, W. L., Meier, M., Oberli, F., et al. (1995). Three natural zircon standards for U-Th-Pb, Lu-Hf, trace element and REE analyses. *Geostandards Newsletter*, *19*(1), 1–23. https://doi.org/10.1111/j.1751-908X.1995.tb00147.x

Wu, F.-Y., Yang, Y.-H., Xie, L.-W., Yang, J.-H., & Xu, P. (2006). Hf isotopic compositions of the standard zircons and baddeleyites used in U-Pb geochronology. *Chemical Geology*, *234*(1), 105–126. https://doi.org/10.1016/j.chemgeo.2006.05.003

Xie, L., Zhang, Y., Zhang, H., Sun, J., & Wu, F. (2008). In situ simultaneous determination of trace elements, U-Pb and Lu-Hf isotopes in zircon and baddeleyite. *Chinese Science Bulletin*, *53*(10), 1565–1573. https://doi.org/10.1007/s11434-008-0086-y

Xiong, X. L., Adam, J., & Green, T. H. (2005). Rutile stability and rutile/melt HFSE partitioning during partial melting of hydrous basalt: Implications for TTG genesis. *Chemical Geology*, *218*(3–4), 339–359. https://doi.org/10.1016/j.chemgeo.2005.01.014

Xiong, X. L., Keppler, H., Audétat, A., Ni, H., Sun, W., & Li, Y. (2011). Partitioning of Nb and Ta between rutile and felsic melt and the fractionation of Nb/Ta during partial melting of hydrous metabasalt. *Geochimica et Cosmochimica Acta*, *75*(7), 1673–1692. https://doi.org/10.1016/j.gca.2010.06.039

Yang, Y., Ritzwoller, M. H., Zheng, Y., Shen, W., Levshin, A. L., & Xie, Z. (2012). A synoptic view of the distribution and connectivity of the mid-crustal low-velocity zone beneath Tibet. *Journal of Geophysical Research: Solid Earth*, *117*(B4). https://doi.org/10.1029/2011JB008810

Yang, Y.-H., Wu, F. Y., Xie, L.-W., Yang, J. H., & Zhang, Y. B. (2009). In situ Sr isotopic measurement of natural geological samples by LA-MC-ICP-MS. *Acta Petrologica Sinica*, *25*(12), 3431–3441. (in Chinese with English abstract).

Yang, Y.-H., Wu, F.-Y., Yang, J.-H., Chew, D. M., Xie, L.-W., Chu, Z.-Y., et al. (2014). Sr and Nd isotopic compositions of apatite reference materials used in U-Th-Pb geochronology. *Chemical Geology*, *385*, 35–55. https://doi.org/10.1016/j.chemgeo.2014.07.012

Zhang, Y.-X., Tang, X.-C., Zhang, K.-J., Zeng, L., & Gao, C.-L. (2013). U-Pb and Lu-Hf isotope systematics of detrital zircons from the Songpan-Ganzi Triassic flysch, NE Tibetan Plateau: Implications for provenance and crustal growth. *International Geology Review*, *56*(1), 29–56. https://doi.org/10.1080/00206814.2013.818754

Zhao, J.-H., Zhou, M.-F., Wu, Y.-B., Zheng, J.-P., & Wang, W. (2019). Coupled evolution of Neoproterozoic arc mafic magmatism and mantle wedge in the western margin of the south China craton. *Contributions to Mineralogy and Petrology*, *174*(4), 36. https://doi.org/10.1007/s00410-019-1573-7